ACS OMEGA

http://pubs.acs.org/journal/acsodf

Article

Insight into the Enhanced Removal of Water from Coal Slime via Solar Drying Technology: Dewatering Performance, Solar Thermal Efficiency, and Economic Analysis

Xin Guo, Kan Li, Pin Zhou, Jianxing Liang, Jia-nan Gu, Yixin Xue, Mingming Guo,* Tonghua Sun,* and Jinping Jia

Cite This: *ACS Omega* 2022, 7, 6710−6720

Read Online

ACCESS | Metrics & More | Article Recommendations | Supporting Information

ABSTRACT: In this work, solar drying technology was applied for the deep dewatering of coal slime to save thermal energy and reduce the dust produced during the hot drying process of coal slime. Solar drying technology is used to dry coal slime to realize its resource utilization. The influence of solar radiation intensity and slime thickness is investigated on the drying process. The greater the solar radiation intensity (SRI) is, the faster the drying indoor air and coal slime are heated, and the faster the drying efficiency is. As the slime becomes thinner, the internal water diffusion resistance becomes smaller and the drying efficiency correspondingly becomes faster. In addition, to facilitate the application of coal slime drying in the actual project, the Page model is fitted and found to have a good fit for solar drying coal slime. Meanwhile, the optimal drying conditions are determined by analyzing the energy utilization under different conditions. It is found that the target moisture content of 10% is optimal for coal slime drying with the highest energy utilization. The laying thickness (L) of 1 cm has the highest solar thermal efficiency of 54.1%. More importantly, economic calculation and analysis are conducted in detail on solar drying. It is found that the cost of solar drying (¥38.59/ton) is lower than that of hot air drying (¥ 65.09/ton). Therefore, solar drying is a promising method for the drying of coal slime.

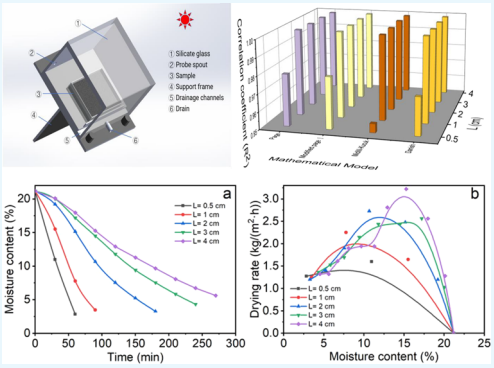

1. INTRODUCTION

Coal slime is a common byproduct during coal processing, and the output of coal slime increased sharply with the increase in coal demand, the continuous improvement of coal mining mechanization, and the continuous development of mineral processing.[1,2] However, coal slime is mainly composed of coal, coal gangue, clay, and water and has many features such as high moisture content, high viscosity, strong ability to combine water, and low calorific value, resulting in environmental pollution and energy waste.[3,4] In recent years, researchers have developed many ways to convert wet slime directly into applications. It can not only reduce environmental pollution but also turn waste into treasure.[3,5−7] Although slime can be utilized in the above methods, the utilization efficiency is low and the effective reduction of coal slime is not successfully realized. Therefore, it is necessary to find a more suitable method of utilizing coal slime.

Coal slime can be used as a fuel due to its calorific value of 2000−4000 kcal/kg, and with the continuous improvement of combustion technology, coal slime can be fully utilized in a well-designed circulating fluidized bed boiler.[8−10] However, moisture has a great influence on the boiler, and it is essential to dry the slime before burning. Flotation, filtration, and dehydration technology can achieve solid−liquid separation but still cannot meet the combustion requirements.[11−18] Therefore, it is of great significance to develop an efficient deep dewatering technology of coal slime.

At present, hot drying technology is usually used for deep dewatering and it can be divided into the conventional method such as hot air drying and the novel drying method (e.g., microwave drying).[19,20] However, hot air drying and microwave drying need primary energy or secondary energy, resulting in high energy consumption, high construction investment, a large amount of dust, a complicated operation, and low safety performance.[21] Therefore, it is of importance to develop green renewable energy to replace thermal energy. Among them, solar energy is considered one of the most environmentally friendly and clean energy sources, and it can be widely used for cooling and heating.[22−24] Solar thermal technology can convert energy into heat, which is widely used

Received: November 4, 2021
Accepted: February 2, 2022
Published: February 15, 2022

https://doi.org/10.1021/acsomega.1c06197
ACS Omega 2022, 7, 6710−6720

in heating or drying industries.[25] Hii et al. used ventilated ovens and solar dryers to simulate the artificial and natural drying process of cocoa beans, Badaoui et al. used a solar greenhouse to dry tomatoes. The application range of solar drying objects continues to expand.[26−28] Various solar energy systems have also been developed and applied, and the corresponding drying model is constantly proposed and improved.[29,30] Meanwhile, solar drying was used in sludge drying to save energy and control pollution. Ameri et al. investigated the application of direct and indirect natural convection solar drying thin-layer tests on Algerian sewage sludge.[31] Wang et al. proposed a new solar sandwich-like chamber drying method, which has a significant effect on sludge drying.[32] Danish et al. studied the drying kinetics and energy parameters of untreated and chemically treated sludge and proposed a new Danish model for the solar drying of sludge.[33]

Hence, the solar drying method was applied for the deep dewatering of coal slime to save thermal energy and reduce the dust produced during the hot drying process of coal slime in this work. The properties of coal slime and the effect of solar radiation intensity (SRI) and laying thickness (L) on the dewatering of coal slime are studied. Moreover, the mathematical fitting, drying kinetics, and energy efficiency analysis of dewatering of coal slime via the solar drying method were deeply investigated. In addition, cost accounting and economic benefit analyses were carried out.

2. RESULTS AND DISCUSSION

2.1. Physicochemical Analyses. *2.1.1. Absorbance Analysis.* As shown in Figure 1, it can be found that the

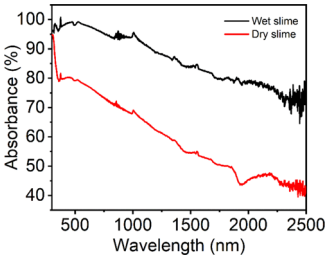

Figure 1. The light absorption of coal slime.

light absorption rate of coal slime is very high. In the visible band, the light absorption rate of wet coal slime is more than 92%, and it can reach about 98% at 500 nm. The overall trend is that the shorter the wavelength of light is, the higher the absorption rate of coal slime is, which makes coal slime absorb a large amount of energy in the visible light band for solar drying.

2.1.2. Thermogravimetric/Differential Thermal Analysis (TGA/DTA). As can be seen from Figure 2, the quality of slime begins to decline significantly at 55 °C, tends to be flat after 116 °C, and then gradually declines after 335 °C. At 116 °C, 20.28% of the weight of coal slime was lost mainly due to adsorbed water and other volatile substances; the second content decline occurred after 360 °C. There is no obvious quality change around 180 °C, which shows that the water content in coal slime mainly exists in the form of free water and the bound water content is minimal.

2.1.3. Particle Size Distribution Analysis. The particle size of coal slime is fine, among which the particles below 10 μm

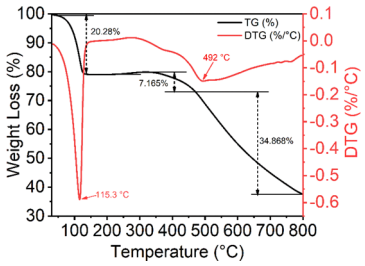

Figure 2. Thermogravimetric/differential thermal curve of coal slime.

account for 74.71% (Table 1). The excessively fine coal slime makes the water storage capacity of coal slime stronger, and the water between particles is difficult to remove.

Table 1. Particle Size Distribution of Coal Slime

size (μm)	145	30	10	5	3	1
pass (%)	100	89.40	74.71	56.29	39.92	13.26

2.2. Drying Characteristics. The drying process is a process in which the object absorbs enough heat from the outside environment so that the moisture contained in it is constantly transferred to the environment, thus leading to the continuous reduction of its moisture content. The process involves heat exchange and mass exchange. To represent these transfer motions, there are a number of typical curves called "drying curves".[34,35] Each product has a drying curve that describes its drying properties under specific conditions.[27]

2.2.1. The Influence of SRI on Coal Slime Drying. It can be seen from Figure 3a that the moisture content in the slime

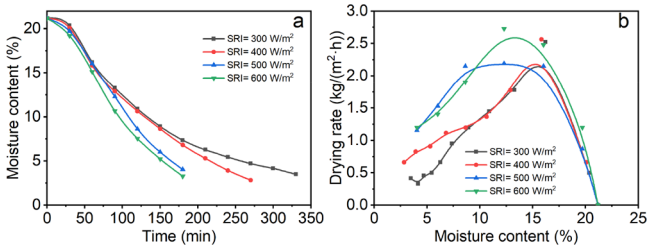

Figure 3. (a) Moisture content change curve under different SRIs and L = 2 cm. (b) Drying curve of coal slime under different SRIs and L = 2 cm.

decreases significantly over time. In the case of the same L, the higher the SRI is, the faster the drying speed is. When the SRI is 300, 400, 500, and 600 W/m^2, it takes about 263, 216, 165, and 150 min for the slime moisture content to be below 5%. In addition, Figure 3b shows that in the process of solar drying of slime, the drying rate and SRI are positively correlated. The drying curve shows that the duration of the constant-rate drying stage is relatively short. When the moisture content of slime decreases from 22.18 to 15%. Then it enters the stage of falling-rate drying, and the period of falling-rate drying rate is long.

During the solar drying process, it is necessary to transfer heat from the air to the slime, and the change of mass and temperature occurs during drying.[36] After the irradiation is turned on, the temperature rises rapidly to above 50 °C within 10 min. Due to the existence of the sampling interval, the temperature of the air in the drying chamber decreases slightly

https://doi.org/10.1021/acsomega.1c06197
ACS Omega 2022, 7, 6710−6720

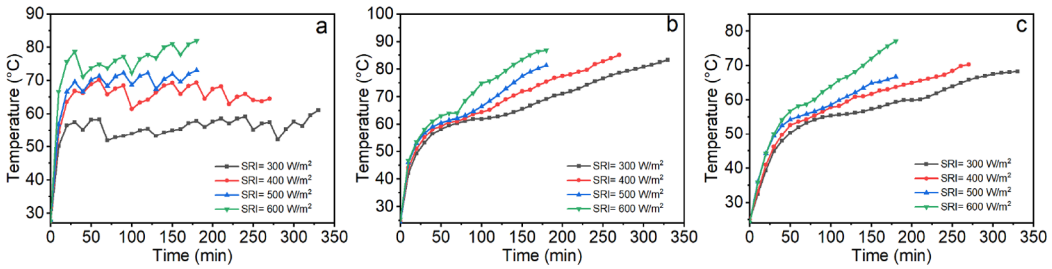

Figure 4. (a) Air temperatures of the drying chamber,(b) surface slime temperatures, and (c) bottom slime temperatures at different SRIs under L = 2 cm.

because of the heat exchange between the air inside and outside the drying chamber, but the temperature tends to be stable on the whole. The maximum temperature of 300, 400, 500, and 600 W/m^2 is 61.2, 66.9, 73.1, and 82.0 °C. The heat for drying slime comes from the solar radiation passing through the glass cover and the heated internal air, so SRI determines the drying efficiency. The air in the drying chamber is heated after being irradiated, and the hot air exchanges heat with the slime to heat up the slime. However, because the moisture concentration gradient is opposite to the temperature gradient, the slime is heated unevenly, and the temperature difference between the surface and the bottom of the slime is large. From Figure 4a,b, it can be seen that the overall temperature of the slime increases with the drying process and the increase in SRI, and the sampling operation has no effect on the temperature rise of the slime. In the first 30 min, the surface temperature of the slime can reach 50 °C, and the bottom temperature is also higher than 45 °C. In this rapid heating stage, the influence of SRI on slime temperature is not obvious, and the difference in slime temperature in various regions is not obvious. After the drying time reaches 1 h, the heating rate of the slime becomes slower and enters a slow heating stage. After 1.5 h, the temperature difference began to become apparent. During the drying time of 3 h, the difference in the surface temperature of coal slime per 100 W/m^2 exceeded 5.4 °C, and the difference in the bottom temperature exceeded 3.1 °C. However, as the drying experiment progressed, the water content in the slime gradually decreased, and the surface temperature of the slime were approachable. The maximum temperature difference on the surface under different irradiation intensities is small, and the temperature difference between the surface layer and the bottom layer is also very close. The change trend of coal slime temperature shows that the water content of coal slime determines the temperature of coal slime.

2.2.2. The Influence of Laying Thickness on the Drying of Slime. Under the same irradiated surface area, the moisture content increases as the L of the slime increases, and the growth and drying rate is higher, which is beyond doubt. The turning point between the constant-rate drying stage and the reduced-rate drying stage is called the critical point, also known as the first critical point, which represents the turning point when the drying rate changes from surface vaporization control to inward diffusion control. The water content of the material at the critical point is called the critical water content (X_C). It can be seen from Figure 5b that when L is 0.5, 1, 2, 3, and 4 cm, the X_C values are 6.25, 8.33, 11.52, 12.06, and 14.92%, respectively. The higher the X_C is, the earlier the drying process will shift to the slow drying stage, which will make the drying time longer, which not only affects product

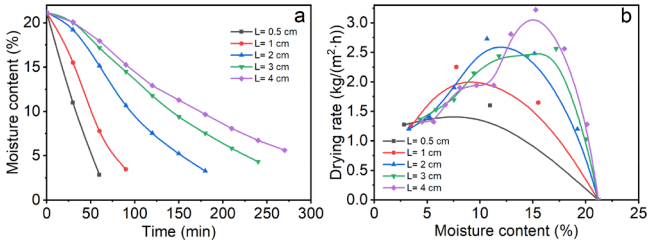

Figure 5. (a) Change curve of moisture content under different L's and SRI = 600 W/m^2. (b) Drying curves of different L's and SRI = 600 W/m^2.

quality but also increases operating costs. In the actual production operation, the drying area can be increased and the critical water content can be reduced by reducing the particle size of the material, reducing the width of the material layer, and stirring the material layer.

Bennamoun et al. proposed that there is an adaptation stage at the beginning of the drying process, which corresponds to the growing-rate drying stage in this experiment.[37] In this stage, the air in the drying chamber is heated, and the temperature of the slime rises after being heated. After about 1 h, the heat absorbed by the slime and the heat consumed by evaporation reach a balance. At this stage, the water content does not decrease much, and after the dehydration rate reaches the maximum, it enters the constant-rate drying stage. Generally speaking, free water is excluded in this stage, and interstitial water is excluded in the first stage of falling-rate drying. In this study, it is found that during the solar drying period of coal slime, the constant-rate drying stage existed for a short time, while the falling-rate drying stage existed for a long time. The main reason for this phenomenon is that the coal slime used in the experiment is the coal slime that has been filtered by a plate and frame filter press, and its free water content is not high. In addition, due to the small particle size of coal slime, the water content between particles is higher. The phenomenon that there is no constant-rate drying period due to the lack of free water on the product surface also appeared in the study of Masmoudi et al.[38]

The L of coal slime has a great influence on the air temperature in the drying chamber. When the SRI is 600 W/m^2 and the drying time is 0.5 h, the temperature difference between the drying chambers with L's of 0.5 and 4 cm is 30 °C. After 1 h, the temperature change tends to be flat, but the air temperature gap is still large. The heat exchange between air and coal slime affects the change of air temperature. It can be seen from Figure 6b,c that the L of slime has a great influence on the temperature of the slime. In the first 20 min of drying, the slime heats up rapidly, and then the temperature rise rate tends to be flat, and the temperature difference under

https://doi.org/10.1021/acsomega.1c06197
ACS Omega 2022, 7, 6710−6720

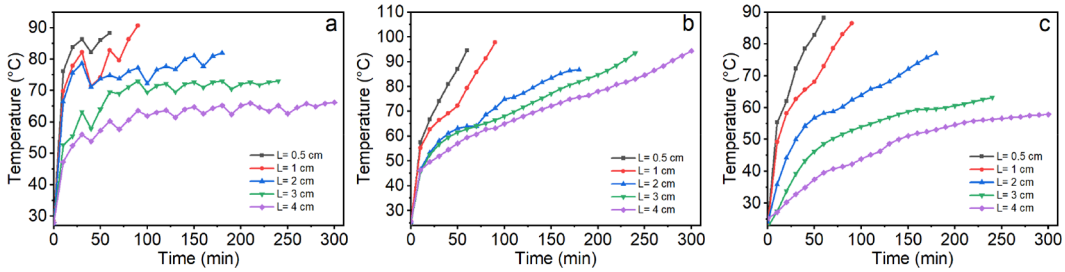

Figure 6. (a) The air temperature of the drying chamber of different L's of slime and SIR = 600 W/m^2. (b) The surface temperature of the slime of different L's and SIR = 600 W/m^2. (c) The bottom temperature of the slime of different L's and SIR = 600 W/m^2.

various L conditions begins to widen. At 1 h, the difference between the surface temperature of 0.5 and 4 cm slime is 34 °C, and the difference of the bottom temperature is 23 °C. What is more obvious is that with the progress of the drying experiment, the final temperature difference on the surface of the slime is not big, but the temperature difference at the bottom is obvious. The maximum temperature difference between the surface and the bottom can reach 36.5 °C. Uneven distribution of moisture and the formation of concentration gradients have an adverse effect on the drying process. Therefore, in practical applications, we should try to make the water distribution even or take measures that are conducive to the diffusion of water.

In addition, when the drying time is 0.5 h, cracks gradually appear on the surface of the slime. The moisture in the surface layer of coal slime evaporates rapidly after being heated, forming a relatively hard shell. When the drying time reaches 1 h, the shell layer is more obvious, and the slime stratification phenomenon is more intuitive. The upper slime becomes gray and has a small moisture content. The coal slime in the lower layer is black with a large water content, and there are obvious water droplets at the bottom. Due to the existence of the shell, the heat and water distribution is not uniform, and the slow drying phase follows. Another obvious phenomenon in the experiment is that there is an obvious water mist on the silicate glass at 0.5 h. With the evaporation of water, the water mist becomes water droplets, making the light transmittance of silicate glass and solar energy utilization efficiency decreased.

2.3. Evaluation of the Models. The change of water content and time is converted into a change of water proportion (MR) and time by using eq 7. The MR and time data are substituted into each equation in Table 6, and the software Origin Pro is used for fitting. The nonlinear regression can evaluate the mathematical model tested and is well adapted to the experimental data.[31] After fitting each model, the infinite constants (a, b, c, and n); the drying rate constants (k, k_0, k_1, g, and h); and the R^2, SSE, RMSE, and χ^2 values between the predicted and experimental values are shown in Figure 7 and Table S2.

Table 2 shows the experimental model results under different SRIs when the L is 2 cm. R^2, SSE, RMSE, and χ^2 values are calculated and compared. The regression coefficients (R^2) of Lewis, Page, Henderson and Pabis, Wang and Singh, and Modified Henderson and Pabis are lower than the results of Wang's simulation of the solar ablation.[32] The common solar ablation model has high applicability to slime drying, and the R^2 of all models is greater than 0.90000. Among all the models, the Newton, Modified Page II, and Henderson and Pabis models show poor-fitting degrees. The maximum R^2 of the Newton model is 0.97660 and the minimum is 0.92030 in

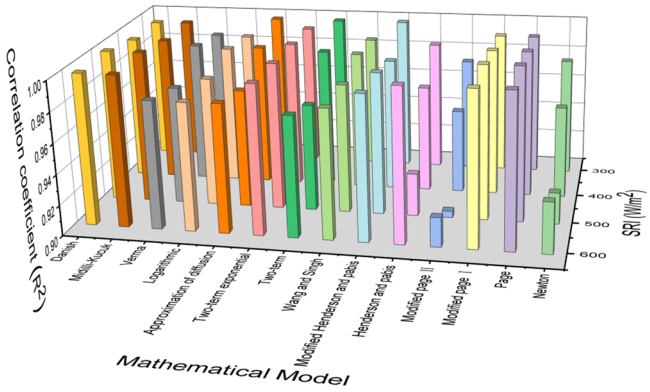

Figure 7. Evaluation of coefficients of correlation for 14 models.

Table 2. The Relationship between the Diffusion Coefficient and SRI of Coal Slime

SRI (W/m^2)	$\frac{\pi^2 D_{eff}}{4l^2}$/min	D_{eff} (m^2/s)	R^2
300	0.006	4.05×10^{-9}	0.9963
400	0.0074	5.00×10^{-9}	0.954
500	0.0082	5.54×10^{-9}	0.9457
600	0.0099	6.69×10^{-9}	0.9454

each condition. Modified Page II is at most 0.97407 and at least 0.90421. The maximum value of Henderson and Pabis is 0.99921, and the minimum value is 0.92757. Combined with SSE, RMSE, and χ^2 values, it is found that the Modified Page II model has the worst fitting effect. Among many models, the models with a high fitting degree are the Page, Modified Page I, Midilli−Kucuk, and Danish models. In each condition, the maximum R^2 values are 0.99979, 0.99979, 0.99967, and 0.99975. The minimum R^2 values are 0.99240, 0.99243, 0.99478, and 0.99464. It can be seen that the worst fitting degree of these models is higher than 0.99000, and the fitting degree of these models for slime drying is higher than that for sludge drying in the presence of sludge, poultry slaughterhouse sludge (PAS), and sludge drying in the presence of CaO and NaClO.[32,33,36] Combined with SSE, RMSE, and χ^2 values, it is found that the Midilli−Kucuk model had the best fitting effect. Its maximum SSE value is 4.02×10^{-3}, the maximum χ^2 value is 5.87×10^{-4}, and the maximum RMSE value is 1.88×10^{-2}.

The model fits of thin coal slime layers under different SRIs are compared, and four models with a high degree of fit are determined. The drying data of coal slime with different L's with an SRI of 600 W/m^2 are substituted into the above four models to determine the most suitable model for coal slime

https://doi.org/10.1021/acsomega.1c06197
ACS Omega 2022, 7, 6710−6720

drying at different L's, and the fitting conditions are shown in Figure 8 and Table S3.

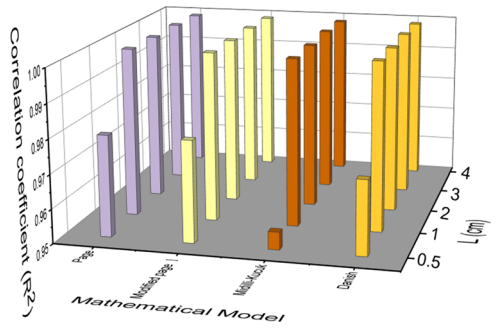

Figure 8. Correlation coefficient evaluation of four models.

In the previously selected four models with a good fit, the fit of different L's with the SRI is compared. It is found that the Midilli−Kucuk model has the lowest fit for 0.5 cm thick slime. Comparing the R^2 data of the other three models, it is found that the model with the highest fit is the Page and Modified Page I models, and the fit can reach more than 0.979. In the future solar thin-layer drying application of coal slime, theoretical calculations can be made through these two models to provide foundation and assistance for subsequent experimental research and reduce drying procedures.

2.4. Effective Diffusivity. The movement of water from the inside to the surface of a product is a complex process resulting from the interaction of multiple mechanisms.[38] Drying kinetics are regularly applied to describe the mechanism of mass and heat transfer in the drying process.[39] The effective diffusion coefficient is an important physical property in the simulation of drying processes. It describes the mass transfer characteristics in porous media and is a function of the temperature and water content of the material.[40] It is assumed that the diffusion coefficient is independent of concentration and the mass transfer surface is a semi-infinite thin layer of semiconductor.[41] If the boundary conditions are used for simplification, the analytical solution of the second Fick's law is

$$\mathrm{MR} = \frac{8}{\pi^2}\sum_{n=1}^{\infty}\frac{1}{(2n+1)}\exp\left[\frac{-(2n+1)^2 \times D_{\mathrm{eff}} \times t}{4l^2}\right] \quad (1)$$

where n is the number of terms taken into account and l is the half slice thickness (m). When the drying time is long enough, all series terms are negligible in comparison with the first term, so eq 1 can be deduced as follows:

$$\mathrm{MR} = \frac{8}{\pi^2}\exp\left(-\frac{\pi^2 \times D_{\mathrm{eff}} \times t}{4l^2}\right) \quad (2)$$

Take the logarithm of both sides of eq 2 to get

$$l_n(\mathrm{MR}) = l_n\left(\frac{8}{\pi^2}\right) - \left(\frac{\pi^2 \times D_{\mathrm{eff}}}{4l^2}\right) \times t \quad (3)$$

It can be seen that the effective diffusion coefficient D_{eff} is the slope of the curve obtained by doing a curve of the l_n(MR) value and drying time (t). The drying effect is positively correlated with the D_{eff} value.

Table 2 shows the D_{eff} values of slime with an L of 2 cm under different SRI conditions. With the increase of SRI, the value of the effective diffusion coefficient D_{eff} also increases. This indicates that the increase of SRI has a positive effect on the desiccation of coal slime. The reason is that the increase of SRI can accelerate the heat exchange between air and coal slime in the drying chamber and accelerate the desiccation process.

Table 3 shows the D_{eff} values of different L's when SRI is 600 W/m^2. It can be seen that the drying time is proportional

Table 3. The Relationship between the Diffusion Coefficient and the L during the Drying Process of Coal Slime

L (cm)	$\frac{\pi^2 D_{\mathrm{eff}}}{4L^2}$/min	D_{eff} (m^2/s)	R^2
0.5	0.0372	1.57×10^{-9}	0.9437
1	0.0207	3.50×10^{-9}	0.9509
2	0.0099	6.69×10^{-9}	0.9454
3	0.0064	9.73×10^{-9}	0.9582
4	0.0046	1.24×10^{-8}	0.9791

to the square of L of the thin layer material and the D_{eff} value is proportional to L. L is positively correlated with the D_{eff} value. Because the L of coal slime increases, the total amount of water contained in the same dry surface area also increases, and the weight loss of water per unit time becomes more obvious.

2.5. Solar Thermal Efficiency Analysis. *2.5.1. Thermal Efficiency Analysis Method.* For the solar drying technology, the goal is to maximize the use of solar energy and evaporate water at the greatest rate under a certain amount of solar light. The reduction of moisture per unit energy is defined as the reduction of specific moisture to evaluate the utilization rate of solar energy when coal slime is dried under different conditions. The calculation method is shown in eq 4:

$$e = \frac{\Delta m}{Q} \quad (4)$$

where e is the specific moisture reduction (kg[H_2O]/J), Δm is the mass of the reduced moisture in the sample (g), and Q is the solar radiant heat received by the drying chamber (J).

The specific moisture reduction can reflect the reduction of moisture during the drying process, but it cannot indicate the solar thermal efficiency. Therefore, the solar thermal efficiency should be calculated according to the reduction of moisture during the drying process and the temperature change. The specific calculation method is as follows:

$$\eta = \frac{Q_e}{Q} = \frac{C_{\mathrm{W}} \times \Delta m \times \Delta T_{\mathrm{W}} + H_{\mathrm{W}} \times \Delta m + C_{\mathrm{S}} \times m_{\mathrm{t}} \Delta T_{\mathrm{S}}}{A \times E \times \alpha \times t} \quad (5)$$

where η is the solar thermal efficiency (%); Q_e is the effective heat gain of the drying chamber (J); C_{W} is the specific heat capacity of water (4183 J/(kg·°C)); ΔT_{W} is the temperature rise of water during the drying process (°C); H_{W} is the latent heat of evaporation of water (J/g); C_{S} is the specific heat capacity of the residual sample (J/(kg·°C)), which changes with water content in the slime; m_{t} is the residual sample mass (g); ΔT_{S} is the temperature rise of coal slime during the drying process (°C); A is the effective radiation area of the drying

https://doi.org/10.1021/acsomega.1c06197
ACS Omega 2022, 7, 6710−6720

chamber (in this experiment, $A = 0.0318 + 0.0318 \times \cos 37° = 0.05614\ m^2$); E is the SRI (W/m^2); α is the light transmittance of silicate glass, which is 90% in this experiment; and t is the drying time (s).

The solar radiation heat received by the drying chamber is mainly used for the temperature rise of water, the evaporation of water, the heat consumption of the sludge temperature rises, and the heat loss of the drying chamber. In this study, the increase in the temperature of coal slime in the drying chamber, the increase in moisture, and the decrease in moisture are measured to calculate the solar thermal efficiency. Since the heat dissipation loss of the drying chamber is negligible compared with the energy loss used for dehydration, the heat dissipation loss of the drying chamber is not included in the calculation.

2.5.2. The Influence of Solar Radiation Intensity on Solar Thermal Efficiency. The effects of SRI and slime L on solar energy utilization under different target moisture contents are investigated. Target moisture contents of 20, 15, 10, and 5% are used to represent the growing-rate, constant-rate, and falling-rate drying stage.

When the L of the slime is 2 cm, the general relationship between the SRI and the specific moisture reduction is as follows: with the increase of the SRI, the specific moisture reduction decreases. In the case of different target water contents, the amount of specific water reduction is not the same. Among them, the maximum reduction of specific water content is the target water content of 10% and the minimum is the target water content of 20%. When the target moisture content is 20%, the reduction of water is the least and the utilization rate of solar energy is the lowest because, at this time, the coal slime is in the initial stage of drying, and the air and coal slime in the drying chamber have not been heated and warmed up. The reason why the target moisture content of 10% is better than 15% can be seen in Figure 3. When the moisture content is 15%, the coal slime is still in the rising drying period or has just crossed this period. The preheating of the coal slime has just finished. The surface of the coal slime is still very wet and in the drying stage controlled by surface vaporization. When the moisture content is 10%, the slime has completely entered the drying period. The surface of coal slime is not wet, and there are some dry local areas and even cracks. Water gradually migrates from the inside of the slime to the surface, and most of the water in the slime is removed in this period, resulting in the highest solar heat utilization rate. When the moisture content is further reduced to 5%, the residual moisture in the slime is reduced, and most of the heat energy is dissipated out of the drying chamber as heat loss, which reduces the heat utilization rate.

Most of the heat is used for the evaporation of water and the heating of residual slime, and the evaporation of water accounts for the largest part of heat. The solar thermal efficiency reaches its maximum before 1 h of drying. The reason is that the high moisture content of coal slime in the early stage makes its specific heat capacity large, which is beneficial to absorb solar radiation. In addition, the color of slime in the early stage is dark, and the absorption rate of sunlight can reach more than 90%, which can be converted into heat energy to a large extent so that the slime can be heated. Combined with Figures 9 and 10, it is found that solar thermal efficiency and specific moisture reduction show the same trend, both of which decrease with the increase of SRI. Due to the large viscosity, small particle size, strong water

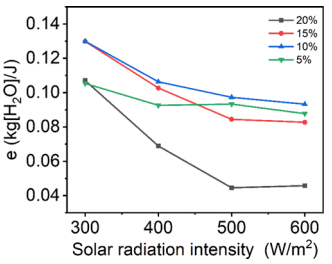

Figure 9. The relationship between specific moisture reduction and SRI under different target moisture contents.

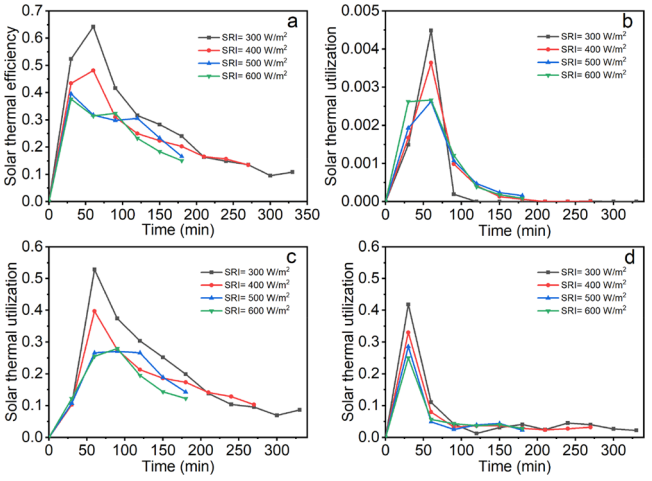

Figure 10. (a) The change of solar thermal efficiency with time under different SRIs. (b) Solar heat utilization due to rising water temperature. (c) Utilization rate of solar energy for water evaporation. (d) Utilization rate of solar energy from coal slime heating.

storage capacity, and small internal water diffusion rate of coal slime, the water diffusion is stable. The absorption rate of the coal slime to solar energy is limited. Therefore, although the rise of SRI can accelerate the evaporation of water and the heating of the coal slime to a certain extent, more heat is absorbed by the air in the drying chamber. As can be seen from Figure 4, under different SRIs, the temperature difference of coal slime is not as big as that of air temperature before 1 h. The temperature of the air in the drying chamber tends to balance after 0.5 h, while the temperature of coal slime is still increasing. This indicates that there is a certain amount of heat exchange between the drying chamber and the external environment. Furthermore, the higher the temperature in the drying chamber is, the greater the heat exchange is; that is, the greater the heat loss is. Therefore, the thermal efficiency of coal slime decreases with the increase of SRI.

2.5.3. The Influence of Coal Slime Paving Thickness on Solar Thermal Efficiency. Similarly, when the target moisture content is 10%, the amount of specific moisture reduction is the largest. In industrial production, 10% moisture content can be selected as the target moisture content of drying, which can not only ensure the high utilization rate of solar energy but also reduce the treatment time, to reduce the production cost. In addition, it is found that about 10% of the coal slime will form a formed block object. Compared with wet coal slime, the coal slime with 10% moisture content is easy to form, easy to break, and easy to transport. It can be seen from Figures 11 and 12 that the utilization rate of solar energy is higher for the slime of 0.5 and 1 cm, while the utilization rate of slime is the lowest

https://doi.org/10.1021/acsomega.1c06197
ACS Omega 2022, 7, 6710−6720

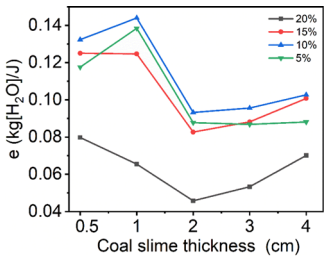

Figure 11. The relationship between specific moisture reduction and slime thickness under different target moisture contents.

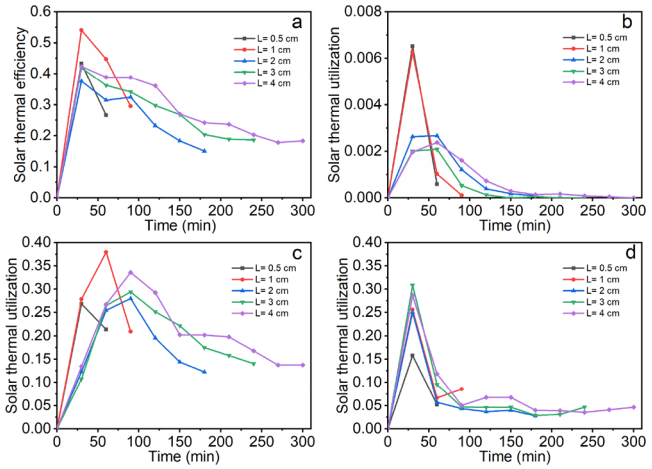

Figure 12. (a) The change of solar thermal efficiency with time under different *L*'s. (b) Solar heat utilization due to rising water temperature. (c) Utilization rate of solar energy for water evaporation. (d) Utilization rate of solar energy from coal slime heating.

when *L* is 2 cm, and the solar thermal efficiency of slime is generally low when *L* is greater than 2 cm. This is because of the formation of the interlayer. When the coal slime is drying, due to uneven heating, the moisture on the surface rapidly diffuses into the air to form a dry area. The internal water cannot be discharged quickly due to the existence of diffusion resistance, so the thicker the slime is, the more obvious the stratification is. However, the *L* of the interlayer on the surface is about 1.3 cm. When *L* is 1 cm, the water diffusion is controlled by surface vaporization, and the resistance of water diffusion is small, so the water evaporation is more obvious. When *L* increases to 2 cm, the water in the interlayer diffuses rapidly, but the water below the interlayer has a greater diffusion resistance. Moreover, the dense and hard interlayer will absorb a large amount of solar energy heat irradiated on its surface, forming an uneven distribution of heat, which results in a large temperature difference between the surface and the bottom of the slime. Therefore, when *L* is greater than 1 cm, the solar thermal efficiency of coal slime is low. Compared with the slime of 3 and 4 cm, the total water content of the slime of 2 cm is less, and the amount of water decrease per unit time is the least. Therefore, the thermal efficiency of the 2 cm slime is the lowest when drying. In actual production, the *L* of 1 cm can be selected to dry water content of 10% to maximize the use of solar energy in the shortest time.

2.6. Economic Calculation Analysis. The operating costs in the process of slime drying are mainly electricity and labor costs in the process of slime transportation. The benefits generated by the drying of coal slime are mainly the saving of a large amount of energy consumption and the energy benefits produced by incineration after the drying of coal slime. Assume that drying equipment is installed in Pingdingshan City, Henan Province. Pingdingshan City is located at 113.29° E, 33.75° N. The *L* of coal slurry is 1 cm, the target moisture content is 10%, and the drying time is from June to October in summer. According to the meteorological data from June to September of 2020, it is found that Pingdingshan City, Henan Province, has favorable SRI in summer. On average, there are 9 days in a month with the highest irradiance greater than 700 W/m^2, 6 days greater than 600 W/m^2, 5 days greater than 500 W/m^2, 5 days greater than 400 W/m^2, and rainy days for 5 days. In the calculation, 16 days of a month are calculated based on the solar radiation intensity of 500 W/m^2 and the working time of 1 day is 10 h; 9 days are calculated based on the solar radiation intensity of 400 W/m^2 and the working time of 1 day is 8 h. In the previous drying experiment, we found that it takes 100, 85, 60, and 50 min for 1 cm slime to dry to a moisture content of 10% under the irradiation of 300, 400, 500, and 600 W/m^2, respectively.

The drying chamber production line occupies an area of 500 m^2 and can process 1551.5 tons of coal slime in 1 month. The operating cost of the slime drying system mainly includes equipment energy consumption, equipment maintenance, investment and construction, and manual maintenance. The energy consumption of the equipment is 100 (kW·h)/day, the electricity cost is calculated at ¥0.56/(kW·h), and the monthly electricity cost is ¥8400. Land purchase is calculated at ¥60/m^2 in Pingdingshan City, and ¥30,000 is required to purchase 500 m^2 of production land. The construction investment cost is ¥1.66 million, and the relevant equipment used in a production line lasts for 10 years and can process approximately 77,575 tons of coal slime. In addition, equipment maintenance costs are calculated at ¥50,000/year, and the cost of drying 1 ton of slime by the solar dryer system is ¥38.59. The cost details of solar drying and hot air drying are shown in Tables S4 and S5. It can be seen from Table 4 that the cost of solar drying is much lower than that of hot air drying.

Table 4. The Cost of Drying 1 Ton of Coal Slime

item	solar drying cost/ton (¥)	hot air drying cost/ton (¥)
land purchase	0.39	0.08
employee salary	10.31	10.31
construction investment	21.40	19.34
equipment maintenance	6.45	6.45
equipment energy consumption	0.04	0.11
steam consumption		28.8
sum	38.59	65.09

The use of solar energy to dry coal slime does not require the use of energy such as coal and natural gas. It saves energy and reduces air pollution caused by the burning of fossil energy, which has good environmental benefits. In addition, the calorific value of coal slime with 10% moisture content is 14.63 MJ/kg. If the power generation efficiency of the circulating boiler fluidized bed is calculated at 36%, the combustion of 77,575 tons of slime can generate 56746.11 kW·h of electricity, which has certain energy benefits.

https://doi.org/10.1021/acsomega.1c06197
ACS Omega 2022, 7, 6710−6720

3. CONCLUSIONS

When using solar energy to dry slime, both the SRI and L of slime will affect the drying process. The greater the SRI is, the faster the drying indoor air and coal slime are heated, and the faster the drying efficiency is. As the thickness of slime becomes thinner, the internal water diffusion resistance becomes smaller and the drying efficiency correspondingly becomes faster.

Through drawing the drying curve, it is found that there is almost no constant-rate drying stage when coal slime is dried, and most of it is in the falling-rate drying stage. Fourteen existing drying models are fitted and compared to determine the most suitable solar drying model for coal slime. The models with the best fit are the Page model and Modified Page I model. In the case of different SRI, the effective diffusion coefficient of water in coal slime varies from 4.05×10^{-9} to 6.69×10^{-9} m^2/s. Under the condition of different L's, the effective diffusion coefficient varies from 1.57×10^{-9} to 1.24×10^{-8} m^2/s.

By calculating the specific moisture reduction and solar thermal efficiency when the slime is dried, it is found that the target moisture content of 10% is optimal for coal slime drying with the highest energy utilization. L of 1 cm has the highest solar thermal efficiency of 54.1%. The cost of drying 1 ton of coal slime by the solar dryer system is ¥38.59, which is lower than that of hot air drying. Meanwhile, the coal slime combustion can generate 56746.11 kW·h of electricity each year, which has good environmental and economic benefits.

4. MATERIALS AND METHODS

4.1. Sample Collection. The coal slime used in the experiment is the dehydrated coal slime from China Pingmei Shenma Group in Pingdingshan City, Henan Province. The coal slime is dehydrated slime treated by a plate and frame filter press, with high viscosity and moisture content of ~21%. The main characteristics of the coal slime data analysis results are shown in Table 5.

Table 5. Main Characteristic Data of Coal Slime Sample

analysis of sludge	parameters and units	value
industrial analysis	M_d (%)	21.18
	A_d (%)	37.69
	V_d (%)	31.80
	FC_d (%)	9.33
elemental analysis	C (%)	43.235
	H (%)	2.881
	N (%)	0.660
	S (%)	0.913
energy analysis	$Q_{b,d}$ (MJ/kg)	13.84

4.2. Dewatering Experiments. The dewatering experiment was carried out in a sandwich dryer with a volume of about 3180 cm^3 ($20.5 \times 15.5 \times 8$ cm^3), and it is topped with a 3 mm thick silicate glass to collect solar energy. The trays and boxes in the drying chamber are made of stainless steel. There is a distance of 2 cm between the bottom of the tray and the shell to keep the water outlet. The sandwich drying chamber was placed at a 37° incline into a SUNTESTR XLS + Artificial Solar Simulator manufactured by Atlas Materials Testing Technology Co., Ltd. A 2.2 kW air-cooled xenon lamp and a solar filter were installed in the simulator to simulate the natural spectral energy distribution (Figure 13).

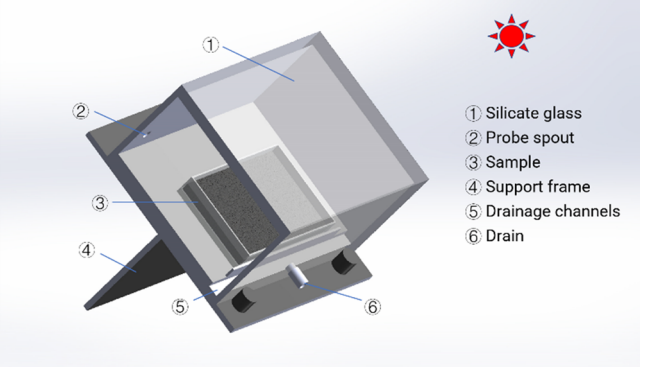

Figure 13. Schematic diagram of the interlayer drying chamber.

4.3. Experimental Procedures. During the experiment, the xenon lamp with a specific illumination intensity emits the light source downward, and the light enters the drying chamber through the silicate glass at the top of the drying chamber, making the air and coal slime in the drying chamber heated up. Then the water in the coal slime overflows and is discharged through the drainage tank. To explore the effect of slime L and SRI on the drying process, five slime L's of 0.5, 1.0, 2.0, 3.0, and 4.0 cm and four SRIs of 300, 400, 500, and 600 W/m^2 were set, respectively. The temperature probe entrance is left in the drying chamber. The air temperature and slime temperature in the drying chamber are tested with a SINO-R200D temperature tester (Sinomeasure), and the temperature change can be controlled within ±1 °C. An electric thermostatic air-blowing drying oven (BPG-9040A Shanghai Yiheng Scientific Instrument Co., Ltd.) was used to measure the initial moisture content of the sludge sample. The weight of slime in the experiment was measured once every 30 min.

4.4. Mathematical Modeling of Drying Curves.

4.4.1. Drying Kinetics. The dried slime was weighed at a specific time to determine the change in moisture content and drying rate during the drying process. The slime and the crucible were put in a 105 °C constant temperature oven for drying to constant to calculate the initial moisture content of the slime. The method of slime moisture content is calculated according to eq 6:[42]

$$M_t = \frac{w_0 - w_t - w_d}{w_d} \tag{6}$$

where M_t is the moisture content at time t (%), w_0 is the initial mass of the slime sample (g), w_t is the weight of water that evaporates at time t (g), and w_d is the dry mass of the slime sample (g).

The normalized moisture ratio (MR) of coal slime at any time in the drying process can be expressed as eq 7:[43]

$$MR = \frac{M_t - M_e}{M_0 - M_e} \tag{7}$$

where M_0 is the initial moisture content of coal slime (%) and M_e is the equilibrium moisture content of coal slime (%). The measured equilibrium moisture content of coal slime in the air is 1.68% in this experiment.

The drying rate of the sample is calculated using eq 8:

https://doi.org/10.1021/acsomega.1c06197
ACS Omega 2022, 7, 6710−6720

$$DR = \frac{M_{t+dt} - M_t}{dt} \quad (8)$$

where M_{t+dt} is the moisture content at time $t + dt$ (%).

4.4.2. Theoretical Models of Drying. Drying is a complex process, with mass and heat transfer in a variety of forms .[42] Several drying models are used for the fitting analysis of experimental data to reveal the relationship between moisture content and time in the process of drying coal slime with solar energy. In this study, 14 common models in Table 6 were used

Table 6. Common Mathematical Models Used to Simulate Solar Drying

model name	model	parameters	refs
Newton	$MR = \exp(-kt)$	k	44
Page	$MR = \exp(-kt^n)$	k, n	45
modified Page I	$MR = \exp(-(kt)^n)$	k, n	46
modified Page II	$MR = \exp((-kt)^n)$	k, n	47
Henderson and Pabis	$MR = a \times \exp(-kt)$	a, k	48
modified Henderson and Pabis	$MR = a \times \exp(-kt) + b \times \exp(-gt) + c \times \exp(-ht)$	a, b, c, k, g, h	49
Wang and Singh	$MR = 1 + at + bt^2$	a, b	50
two-term	$MR = a \times \exp(-k_0 t) + b \times \exp(-k_1 t)$	a, b, k_0, k_1	51
two-term exponential	$MR = a \times \exp(-kt) + (1 - a) \times \exp(-kat)$	a, k	52
approximation of diffusion	$MR = a \times \exp(-kt) + (1 - a) \times \exp(-kbt)$	a, b, k	53
logarithmic	$MR = a \times \exp(-kt) + c$	a, k, c	54
Verma	$MR = a \times \exp(-kt) + (1 - a) \exp(-gt)$	a, k, g	55
Midilli–Kucuk	$MR = \exp(-kt^n) + bt$	a, b, k, n	56
Danish	$MR = \exp(-kt^n) + b$	a, b, k, n	33

for mathematical modeling of slime drying, and the regression method was used to analyze and compare the fitting performance of different models under the same experimental conditions.

4.4.3. Statistical Analysis. The applicability of the theoretical model was evaluated by the mathematical statistics method to determine the degree of fitting between the experimental data and the theoretical model. According to the mathematical statistics, the correlation coefficient (R^2), the sum of square error (SSE), the root mean square error (RMSE), and chi-square (χ^2) values made it possible to directly compare the fitting degree of the model using the corresponding data. The closer R^2 is to 1 and the smaller the other three values are, the better the fitting degree is and the higher the applicability of the model is. The R^2, SSE, RMSE, and χ^2 values can be calculated by the following equations:

$$R^2 = \frac{\sum_{i=1}^{N} (MR_i - MR_{pre,i}) \times (MR_i - MR_{exp,i})}{\sqrt{\left[\sum_{i=1}^{N} (MR_i - MR_{pre,i})^2\right] \times \left[\sum_{i=1}^{N} (MR_i - MR_{exp,i})^2\right]}} \quad (9)$$

$$\chi^2 = \frac{\sum_{i-1}^{N} (MR_{pre,i} - MR_{exp,i})^2}{N - n} \quad (10)$$

$$RMSE = \left[\frac{1}{N} \sum_{i=1}^{N} (MR_{pre,i} - MR_{exp,i})\right]^{1/2} \quad (11)$$

where $MR_{exp,i}$ is the tried water content during the experiment, $MR_{pre,i}$ is the predicted moisture content in the drying model brought in, N is the total number of samples, and n is the number of constants contained in the model.

■ ASSOCIATED CONTENT

Supporting Information

The Supporting Information is available free of charge at https://pubs.acs.org/doi/10.1021/acsomega.1c06197.

IDR of different slime L's (Table S1); fitting situation of coal slime drying model under different SRIs (Table S2); fitting situation of coal slime drying model under different L's (Table S3); the cost of solar drying 1 ton of coal slime (Table S4); and the cost of hot air drying 1 ton of coal slime (Table S5) (PDF)

■ AUTHOR INFORMATION

Corresponding Authors

Mingming Guo − *School of Environmental Science and Engineering, Shanghai Jiao Tong University, Shanghai 200240, P.R. China; Shanghai Engineering Research Center of Solid Waste Treatment and Resource Recovery, Shanghai 200240, P.R. China; Chongqing Research Institute of Shanghai Jiaotong University, Chongqing 401120, P.R. China*; Email: mingmingguo@sjtu.edu.cn

Tonghua Sun − *School of Environmental Science and Engineering, Shanghai Jiao Tong University, Shanghai 200240, P.R. China; Shanghai Engineering Research Center of Solid Waste Treatment and Resource Recovery, Shanghai 200240, P.R. China*; orcid.org/0000-0003-3803-0232; Email: sunth@sjtu.edu.cn

Authors

Xin Guo − *School of Environmental Science and Engineering, Shanghai Jiao Tong University, Shanghai 200240, P.R. China*

Kan Li − *School of Environmental Science and Engineering, Shanghai Jiao Tong University, Shanghai 200240, P.R. China*; orcid.org/0000-0002-1961-2459

Pin Zhou − *Research Center of Secondary Resources and Environment, 666 Liaohe Road, Changzhou Institute of Technology, Changzhou 213032, P.R. China*

Jianxing Liang − *School of Environmental Science and Engineering, Shanghai Jiao Tong University, Shanghai 200240, P.R. China*

Jia-nan Gu − *School of Environmental Science and Engineering, Shanghai Jiao Tong University, Shanghai 200240, P.R. China*

Yixin Xue − *School of Environmental Science and Engineering, Shanghai Jiao Tong University, Shanghai 200240, P.R. China*

Jinping Jia − *School of Environmental Science and Engineering, Shanghai Jiao Tong University, Shanghai 200240, P.R. China; Shanghai Institute of Pollution Control and Ecological Security, Shanghai 200092, P.R. China*; orcid.org/0000-0003-2409-338X

Complete contact information is available at: https://pubs.acs.org/10.1021/acsomega.1c06197

Notes

The authors declare no competing financial interest.

https://doi.org/10.1021/acsomega.1c06197
ACS Omega 2022, 7, 6710−6720

■ ACKNOWLEDGMENTS

This work was supported by the National Natural Science Foundation of China (Grant Nos. 21976119, 21876107, and 22076118), Shanghai Sailing Program (21YF1420800), Startup Fund for Youngman Research at SJTU (21X010500781), and Open funding from Shanghai Engineering Research Center of Solid Waste Treatment and Resource Recovery (2020GFZX006) and sponsored by the Natural Science Foundation of Chongqing, China (cstc2021jcyj-msxmX0252).

■ REFERENCES

(1) He, J.; Zhu, L.; Liu, C.; Bai, Q. Optimization of the oil agglomeration for high-ash content coal slime based on design and analysis of response surface methodology (RSM). *Fuel* **2019**, *254*, 115560.
(2) Wang, H.; Liu, S.; Li, X.; Yang, D.; Wang, X.; Song, C. Morphological and structural evolution of bituminous coal slime particles during the process of combustion. *Fuel* **2018**, *218*, 49−58.
(3) Dai, Z.; Shi, L.; Wang, L.; Guo, C. Rheological behaviors of coal slime produced by filter-pressing. *Int. J. Min. Sci. Technol.* **2018**, *28*, 347−351.
(4) Zhou, K.; Lin, Q.; Hu, H.; Shan, F.; Fu, W.; Zhang, P.; Wang, X.; Wang, C. Ignition and combustion behaviors of single coal slime particles in CO_2/O_2 atmosphere. *Combust. Flame* **2018**, *194*, 250−263.
(5) Tan, J.; Cheng, H.; Wei, L.; Wei, C.; Xing, Y.; Gui, X. Using low-rank coal slime as an eco-friendly replacement for carbon black filler in styrene butadiene rubber. *J. Cleaner Prod.* **2019**, *234*, 949−960.
(6) Meng, Z.; Yang, Z.; Yin, Z.; Li, Y.; Song, X.; Zhao, J.; Wu, W. Effects of coal slime on the slurry ability of a semi-coke water slurry. *Powder Technol.* **2020**, *359*, 261−267.
(7) Guo, H.; Zhao, S.; Xia, D.; Wang, L.; Lv, J.; Yu, H.; Jiao, X. Efficient utilization of coal slime using anaerobic fermentation technology. *Bioresour. Technol.* **2021**, *332*, 125072.
(8) Song, G.; Xiao, Y.; Yang, Z.; Yang, X.; Lyu, Q.; Zhang, X.; Pan, Q. Operating characteristics and ultra-low NO_x emission of 75 t/h coal slime circulating fluidized bed boiler with post-combustion technology. *Fuel* **2021**, *292*, 120276.
(9) Nowak, W. Clean coal fluidized-bed technology in Poland. *Appl. Energy* **2003**, *74*, 405−413.
(10) Fan, H.; Deng, B.; Shi, J.; Qin, S.; Feng, Y.; Huang, Z.; Fan, B.; Yang, H.; Jin, Y.; Zhang, M. Experimental research on morphology and drying characteristics of coal slime dough injected into circulating fluidized bed boiler. *Fuel Process. Technol.* **2021**, *222*, 106981.
(11) Li, L.; Ma, C.; Hu, S.; He, M.; Yu, H.; Wang, Q.; Cao, X.; You, X. Effect of the benzene ring of the dispersant on the rheological characteristics of coal-water slurry: Experiments and theoretical calculations. *Int. J. Min. Sci. Technol.* **2021**, *31*, 515−521.
(12) Liu, S.; Chen, X.; Peng, Y. Destabilising persistent coal froth using silicone oil. *Int. J. Min. Sci. Technol.* **2021**, *31*, 1023−1031.
(13) Lai, Q.; Liao, Y.; Liu, Z. Enhanced low-rank coal slime dewatering by adjustment of channel wall structure and surface wettability. *Sep. Purif. Technol.* **2020**, *248*, 116970.
(14) Li, L.; Ma, C.; Li, Z.; Liu, M.; Lin, M.; He, M.; Wang, Q.; You, X. Role of sodium dodecyl benzene sulfonate in enhancing coal dewatering: Experiments and theoretical calculations. *Drying Technol.* **2020**, 1−10.
(15) You, X.; He, M.; Zhu, X.; Wei, H.; Cao, X.; Wang, P.; Li, L. Influence of surfactant for improving dewatering of brown coal: A comparative experimental and MD simulation study. *Sep. Purif. Technol.* **2019**, *210*, 473−478.
(16) Nguyen, C. V.; Nguyen, A. V.; Doi, A.; Dinh, E.; Nguyen, T. V.; Ejtemaei, M.; Osborne, D. Advanced solid-liquid separation for dewatering fine coal tailings by combining chemical reagents and solid bowl centrifugation. *Sep. Purif. Technol.* **2021**, *259*, 118172.
(17) Vajihinejad, V.; Gumfekar, S. P.; Dixon, D. V.; Silva, M. A.; Soares, J. B. P. Enhanced dewatering of oil sands tailings by a novel water-soluble cationic polymer. *Sep. Purif. Technol.* **2021**, *260*, 118183.
(18) Rostami Najafabadi, Z.; Soares, J. B. P. Flocculation and dewatering of oil sands tailings with a novel functionalized polyolefin flocculant. *Sep. Purif. Technol.* **2021**, *274*, 119018.
(19) Tahmasebi, A.; Yu, J.; Li, X.; Meesri, C. Experimental study on microwave drying of Chinese and Indonesian low-rank coals. *Fuel Process. Technol.* **2011**, *92*, 1821−1829.
(20) Song, Z.; Jing, C.; Yao, L.; Zhao, X.; Sun, J.; Wang, W.; Mao, Y.; Ma, C. Coal slime hot air/microwave combined drying characteristics and energy analysis. *Fuel Process. Technol.* **2017**, *156*, 491−499.
(21) Song, Z.; Jing, C.; Yao, L.; Zhao, X.; Wang, W.; Mao, Y.; Ma, C. Microwave drying performance of single-particle coal slime and energy consumption analyses. *Fuel Process. Technol.* **2016**, *143*, 69−78.
(22) Fudholi, A.; Sopian, K. A review of solar air flat plate collector for drying application. *Renewable Sustainable Energy Rev.* **2019**, *102*, 333−345.
(23) Chuayboon, S.; Abanades, S. Combined ZnO reduction and methane reforming for co-production of pure Zn and syngas in a prototype solar thermochemical reactor. *Fuel Process. Technol.* **2021**, *211*, 106572.
(24) Lingayat, A. B.; Chandramohan, V. P.; Raju, V. R. K.; Meda, V. A review on indirect type solar dryers for agricultural crops − Dryer setup, its performance, energy storage and important highlights. *Appl. Energy* **2020**, *258*, 114005.
(25) Ismail, M. I.; Yunus, N. A.; Hashim, H. Integration of solar heating systems for low-temperature heat demand in food processing industry − A review. *Renewable Sustainable Energy Rev.* **2021**, *147*, 111192.
(26) Hii, C. L.; Law, C. L.; Cloke, M. Modelling of thin layer drying kinetics of cocoa beans during artificial and natural drying. *J. Eng. Sci. Technol.* **2008**, *3*, 1−10.
(27) Badaoui, O.; Hanini, S.; Djebli, A.; Haddad, B.; Benhamou, A. Experimental and modelling study of tomato pomace waste drying in a new solar greenhouse: Evaluation of new drying models. *Renewable Energy* **2019**, *133*, 144−155.
(28) Grimm, A.; Etula, J.; Salh, R.; Kalén, G.; Segerström, M.; Brücher, J.; Söderberg, C.; Soukup, D.; Pfeifer, C.; Larsson, S. H. Slagging and fouling characteristics during co-combustion of Scots pine bark with low-temperature dried pulp and paper mill chemical sludge. *Fuel Process. Technol.* **2019**, *193*, 282−294.
(29) Rathore, N. S.; Panwar, N. L. Experimental studies on hemi cylindrical walk-in type solar tunnel dryer for grape drying. *Appl. Energy* **2010**, *87*, 2764−2767.
(30) Tian, Y.; Zhao, C. Y. A review of solar collectors and thermal energy storage in solar thermal applications. *Appl. Energy* **2013**, *104*, 538−553.
(31) Ameri, B.; Hanini, S.; Boumahdi, M. Influence of drying methods on the thermodynamic parameters, effective moisture diffusion and drying rate of wastewater sewage sludge. *Renewable Energy* **2020**, *147*, 1107−1119.
(32) Wang, P.; Mohammed, D.; Zhou, P.; Lou, Z.; Qian, P.; Zhou, Q. Roof solar drying processes for sewage sludge within sandwich-like chamber bed. *Renewable Energy* **2019**, *136*, 1071−1081.
(33) Danish, M.; Jing, H.; Pin, Z.; Ziyang, L.; Pansheng, Q. A new drying kinetic model for sewage sludge drying in presence of CaO and NaClO. *Appl. Therm. Eng.* **2016**, *106*, 141−152.
(34) Ameri, B.; Hanini, S.; Benhamou, A.; Chibane, D. Comparative approach to the performance of direct and indirect solar drying of sludge from sewage plants, experimental and theoretical evaluation. *Sol. Energy* **2018**, *159*, 722−732.
(35) Bennamoun, L.; Arlabosse, P.; Léonard, A. Review on fundamental aspect of application of drying process to wastewater sludge. *Renewable Sustainable Energy Rev.* **2013**, *28*, 29−43.
(36) López-Ortiz, A. N. A. B. E. L.; Pacheco Pineda, I. Y.; Méndez-Lagunas, L. L.; Balbuena Ortega, A.; Guerrero Martinez, L.; Pérez-

https://doi.org/10.1021/acsomega.1c06197
ACS Omega 2022, 7, 6710−6720

Orozco, J. P.; del Río, J. A.; Nair, P. K. Optical and thermal properties of edible coatings for application in solar drying. *Sci. Rep.* **2021**, *11*, 10051.
(37) Bennamoun, L.; Chen, Z.; Salema, A. A.; Afzal, M. T. Moisture diffusivity during microwave drying of wastewater sewage sludge; In *2014 Montreal, Quebec Canada July 13−July 16, 2014*; American Society of Agricultural and Biological Engineers: St. Joseph, MI, p. 1.
(38) Masmoudi, A.; Ali, A. B. S.; Dhaouadi, H.; Mhiri, H. Draining solar drying of sewage sludge: Experimental study and modeling. *Environ. Prog. Sustainable Energy* **2021**, *40*, No. e13499.
(39) Lamidi, R. O.; Jiang, L.; Pathare, P. B.; Wang, Y. D.; Roskilly, A. P. Recent advances in sustainable drying of agricultural produce: A review. *Appl. Energy* **2019**, *233-234*, 367−385.
(40) Masmoudi, A.; Ali, A. B. S.; Dhaouadi, H.; Mhiri, H. Comparison Between Two Solar Drying Techniques of Sewage Sludge: Draining Solar Drying and Drying Bed. *Waste Biomass Valorization* **2021**, *12*, 4089−4102.
(41) Parlak, N.; Ozdemir, S.; Yetilmezsoy, K.; Bahramian, M. Mathematical Modeling of Thin-Layer Solar Drying of Poultry Abattoir Sludge. *Int. J. Environ. Res.* **2021**, *15*, 177−190.
(42) Zhou, Y.; Jin, Y. Mathematical modeling of thin-layer infrared drying of dewatered municipal sewage sludge (DWMSS). *Procedia Environ. Sci.* **2016**, *31*, 758−766.
(43) Kara, C.; Doymaz, O. Effective moisture diffusivity determination and mathematical modelling of drying curves of apple pomace. *Heat Mass Transfer* **2015**, *51*, 983−989.
(44) Onwude, D. I.; Hashim, N.; Janius, R. B.; Nawi, N. M.; Abdan, K. Modeling the thin-layer drying of fruits and vegetables: A review. *Compr. Rev. Food Sci. Food Saf.* **2016**, *15*, 599−618.
(45) Page, G. E. *Factors Influencing the Maximum Rates of Air Drying Shelled Corn in Thin layers.*, Purdue University, 1949.
(46) Overhults, D. G.; White, G. M.; Hamilton, H. E.; Ross, I. J. Drying soybeans with heated air. *Trans. ASAE* **1973**, *16*, 112.
(47) White, G. M.; Ross, I. J.; Poneleit, C. G. Fully-exposed drying of popcorn. *Trans. ASAE* **1981**, *24*, 466−468.
(48) Chhinnan, M. S. Evaluation of selected mathematical models for describing thin-layer drying of in-shell pecans. *Trans. ASAE* **1984**, *27*, 610−615.
(49) Karathanos, V. T. Determination of water content of dried fruits by drying kinetics. *J. Food Eng.* **1999**, *39*, 337−344.
(50) Wang, C. Y.; Singh, R. P. *A single layer drying equation for rough rice*; ASAE paper, 1978.
(51) Doymaz, I. Thin-layer drying behaviour of mint leaves. *J. Food Eng.* **2006**, *74*, 370−375.
(52) Sharaf-Eldeen, Y. I.; Blaisdell, J. L.; Hamdy, M. Y. A model for ear corn drying. *Trans. ASAE* **1980**, *5*, 1261−1265.
(53) Kassem, A. S. Comparative studies on thin layer drying models for wheat. *13th international congress on agricultural engineering*; 1998, 2 −6.
(54) Yagcioglu, A. 13th international congress on agricultural engineeringDrying characteristic of laurel leaves under different conditions. *Proceedings of the 7th International congress on agricultural mechanization and energy, 1999*; Faculty of Agriculture, Cukurova University, 1999, pp. 565−569.
(55) Verma, L. R.; Bucklin, R. A.; Endan, J. B.; Wratten, F. T. Effects of drying air parameters on rice drying models. *Trans. ASAE* **1985**, *28*, 296−301.
(56) Midilli, A.; Kucuk, H.; Yapar, Z. A new model for single-layer drying. *Drying Technol.* **2002**, *20*, 1503−1513.

https://doi.org/10.1021/acsomega.1c06197
ACS Omega 2022, 7, 6710−6720